RESEARCH PAPER | Environment | Volume : 3 | Issue : 7 | July 2013 | ISSN - 2249-555X

Solid state synthesis of $MZrO_3$ (M = Pb, Cd and Cu) photocatalyst-A Green chemistry approach

KEYWORDS: Green chemistry, Photocatalyst, Photodegradation, Direct black dye, SEM, TEM

Ashok Vishram Borhade
Research Centre, Department of Chemistry, Hansraj Pragjee Thackersey Arts and Raojisa Yamasa Kshatriya Science College, Nashik, 422005 Maharashtra, India

Vishwas Bhaskar Gaikwad
Director, Board of College and University Development, University of Pune, Ganeshkhind , Pune, 411007 Maharashtra, India

Yogeshwar Rajaram Baste
Research Centre, Department of Chemistry, Hansraj Pragjee Thackersey Arts and Raojisa Yamasa Kshatriya Science College, Nashik, 422005 Maharashtra, India

ABSTRACT *$MZrO_3$ (M = Pb, Cu and Cd) photocatalyst have been successfully synthesized by mechanochemical – solid state method with green chemistry approach. The synthesized photocatalysts were characterized for microstructural properties by various analytical investigative techniques like, Fourier transform infra red spectroscopy (FTIR), UV-visible diffused reflectance spectroscopy (UV-DRS), Barret, Joyner and Halenda (BJS-BET) surface area, Scanning electron microscopy (SEM), Energy dispersive spectrometer (EDS), Tunneling Electron microscopy (TEM) with Selective area electron diffraction (SAED) Electrical conductivity and Thermogravimetric analysis (TGA). The photocatalytic power of the sample was investigated systematically using direct black dye under different irradiation wavelengths. Solar light was employed as irradiation source showing that this type of structures could drive to plausible strategy for developing photocatalyst to degrade waste-water. The synthesized $PbZrO_3$, $CdZrO_3$ and $CuZrO_3$ shows orthorhombic pervoskite phase with BET surface area, surface area 49.49 m^2/g, 13.60 m^2/g, 20.22 m^2/g, respectively Photodegradation of direct black dye follows pseudo first order kinetic.*

1. Introduction

Environmental contamination, which is growing around world or in our daily life, is serious social problem. Synthetic dyes manufactured each year mainly used in the textile, lather products, industrial painting, food, plastic, cosmetics, and consumer electronic structures. Dye stuffs used all over the places are one of the main classes of contaminants in waste-water, especially those from the textile industry and the photographic industry. A fraction of this dyes are lost during the dying process and released into effluent water streams form the above industries [S. Tsuda et al. 2001). The discharge of colored waste–water in the eco system is a source of non aesthetic pollution and perturbs an aquatic life by increasing serious health-risk factor. Being released into the environment, these dyes not only impart colors to water sources but also damage living organisms by stopping the reoxygenation capacity of water by blocking sunlight, and therefore disturbing the natural growth activity of aquatic life. Therefore, serious efforts to the decolorization and detoxification of dyes effluent must be given before discharge into various water bodies.

Various approaches have suggested for the removal of dye pollutants like, physical, biological, and chemical methods. Garg has removed dyestuff efficiently by adsorption technique [V. K. Garg et al 2003) ultra filtration [Bohdziewicz et al 2003), Gholami and Ohnishi demonstrated reverse osmosis and membrane techniques for removal of dyes from waste-warter [Gholami and Nasser 2001, Ohnishi and Okuno 1998) Moghaddam adopted coagulation technique for removal of dye [Moghaddam et al 2010). In biological method, Slots have removed pollutants by application of special fungi [Stolz 2001). The Chu and Wai used chemical treatment such as chlorination and ozonation (Chu, and Wai 2000). These treatment technologies have proven to be markedly ineffective for handling waste water because of the moderately stability of these pollutants.

Mineralization of pollutants using interaction between ultraviolet - visible radiation and semi-conductor metal-oxide catalysts has a strong potential in the industrial destruction of toxic as it has been widely demonstrated by Manilal (Manilal et al 1992). This technique has fascinated for decontamination of polluted water, for its efficiency and promising economy. The heterogeneous solar degradation process consists of making use of solar spectrum to photo-excite a semiconductor catalyst in contact with water in presence of oxygen. The most important feature of this process to treatment of contaminated water are; the process takes place at ambient temperature, oxidation of substance into CO_2 and other inorganic process is complete. The oxygen required directly obtained from the atmosphere. The energy for photo-excitation of catalyst directly obtained from the sun. The catalyst is low cost, long-term stability, and safe to the environment.

Photocatalyst have been widely applied in various areas such as, antibacterial materials (Diana 2007), degradation of pesticides (Ioannis 2003), degradation of insecticides (Kitsiou and Filippidis 2003), anticancer (Weisburger 2002), degradation of dyes (Borhade and Baste 2012) and Fabiola degraded medicine ibuprofen by photocatalysis (Fabiola 2010). Doggan and Vulliet used TiO_2 degraded organic material by photocatalysis. (Doggan et al 2007, Vulliet and Emmelin 2010) after TiO_2, ZnO is other most studied material for its photocatalytic application (Behnajady 2010). Some reports are available on the studies related to the photocatalytic activity of coupled semiconductor photocatalyst, such as TiO_2-SnO_2 (Tada and Hattori 2000) and ZnO-SnO_2 (C. Wang 2004, W. Wang 2007), Celik used doped metal oxide like, Cu-doped TiO_2 (Celik and Gokcen 2006) and Borhade used Fe doped MgO (Borhade 2012), mixed metal oxide for photocatalysis purpose. Subramanian used mixed metal oxide like $SrTiO_3$ for photocatalysis (Subramanian 2006). Various methods are available for the synthesis of metal oxide photocatalyst such as; hydrothermal sol-gel synthesis (M. Aramendía 2005, Song and Wang 2004), co-precipitation (Zoltan 2008) thin films by spray Pyrolysis (Natarajan et al 1998) and thin film vapor deposition method (Sun, and Akpan 2008). These methods are complicated, cost effective and main disadvantage is that they cause environmental pollution.

In this sense, an interesting approach to deal with pollution is carried out by a green chemistry, solid-state method with mechanochemical synthesis has adopted for preparation of

Volume : 3 | Issue : 7 | July 2013 | ISSN - 2249-555X

metal oxide photocatalyst. There are certain advantages of the solid-state, mechanochemical synthesis method like; it is an environmentally friendly, easy, and low cost method. Also, no additives are required for the synthesis of the compound. It is fast and ecologically pure. The chemical stability of the photocatalyst produced is moderately high.

2. Materials and Methods:

2.1 Synthesis of photocatalyst

The aim of this study is to optimize the preparation for $MZrO_3$ (M= Pb, Cd and Cu) photocatalyst. For that purpose, a solid state-mechanochemical synthesis method, with a green chemistry approach was employed for the synthesis photocatalyst. Starting reagents were of MO (Metal oxide) includes, PbO (Merck, Batch No MD6M561095 CAS No 1314-13-2, 99.9 % pure), CuO (Analytical Reagent, Batch No 92730804, CAS No 1317-38-0, 99.9 % pure). CdO (Sr. no.-361 Batch No 600220109, 99.9 % pure) and ZrO_2 (Sigma Aldrich, Lot no BCBF3242V CAS No 1314-23-4). For the synthesis of $MZrO_3$, equimolar mixture of MO and ZrO_2 was grinded with mortar and pestle to acquire fine powder for 25 min. and calcinated at 500 °C for 3 h. Again, the obtained powder was further calcinated at 800 °C following milling after each interval of three-hour of time. The calcination was continued for next twenty hours with milling. Afterwards, at the end mixture was heated up to the terminal temperature. The furnace was programmed as 10 °C per min from one temperature to subsequent higher temperature. The product $PbZrO_3$, $CuZrO_3$, and $CdZrO_3$ thus obtained, were characterized and utilized to evaluate photocatalytic activity against direct black dye.

2.2. Photodegradation of Direct Black dye

The photocatalytic properties of synthesized photocatalyst were evaluated by photodegradation of the direct black dye on exposure to the sunlight. The experiment was performed in three cases, in case one, to evaluate effect of photocatalyst in presence of sunlight, 0.250 g of $PbZrO_3$ photocatalyst was suspended in 100 mL of 50 mg/L dye solution and exposed to the sunlight. In case two, to evaluate effect of sunlight in absence of photocatalyst, only dye solution was exposed to the sunlight. In third case, to evaluate effect of photocatalyst in absence of light, dye solution containing same amount of photocatalyst was kept in dark. The effect of light/or photocatalyst on dye solution was studied by analyzing aliquots on UV-visible spectrophotometer (950-Perkin-Elmer) at after every 30 min. The change in the sunlight intensity during progress of decolorization with time was monitored on Lux meter. The same procedure was implemented for $CuZrO_3$ and $CdZrO_3$ to evaluated photocatalytic property.

2.3. Characterization of $MZrO_3$ (M= Pb, Cd and Cu) photocatalyst

The vibrational frequency of the synthesized catalyst was studied by FTIR-8400S (Shimadzu) in the range of 400– 4000 cm^{-1}. The optical property of the synthesized product was studied by using UV–visible spectrophotometer-k-950 (Perkin-Elmer) over range of 200-800nm. The structural properties of the material was studied using X-ray diffractometer-DMAX-2500 (Rigaku) with Cu-Kα radiation, with λ = 1.5406 A°. The surface morphology and chemical compositions of synthesized catalyst was analyzed using a Scanning tlectron microscope-JSM-6300 (JEOL) coupled with an Energy dispersive spectrometer-JED-2300LA (JEOL). The TEM images were recorded on Philips model no. CM200. The Surface area (SBET), Pore volume(Vp) and Pore diameter (Dp) was evaluated on Quntachrome autosorb automated gas sorption system, Autosorb-1 NOVA-1200 and Mercury porositymeter autosoeb-IC. Electrical conductivities were measured by using thick films of the synthesized photocatalysts static gas sensing system. For measurement of electrical properties, thick film of the synthesized photocatalyst was used. The effect of temperature on stability of the catalyst was evaluated by thermogravimetric analysis on thermogravimetric analyzer (Perkin Elmer-TG) using Xenon arc lamp. The variation in the sunlight intensity during the experiment was measured by Lux-meter (Kusam-meko, KMLUX).

3. Results and discussion

3.1 Characterization of $MZrO_3$ (M= Pb, Cd and Cu) photocatalyst

Figure 1 shows Infra-red spectra of synthesized $PbZrO_3$, $CdZrO_3$and $CuZrO_3$ photocatalyst. The frequency bands at 420 cm^{-1}, vibrational frequency range at 730 to 760 cm^{-1} and 1104 cm^{-1} indicate Zr-O vibrational frequency, while vibrational frequency band 516 cm^{-1}, 569 cm^{-1} indicates the presence of Pb-O. The vibrational frequency bands at 509, 518 and 1178 cm^{-1} indicates the presence of the Cu–O and 501 cm^{-1}, 995 cm^{-1} confirm presence of Cd-O vibrations.

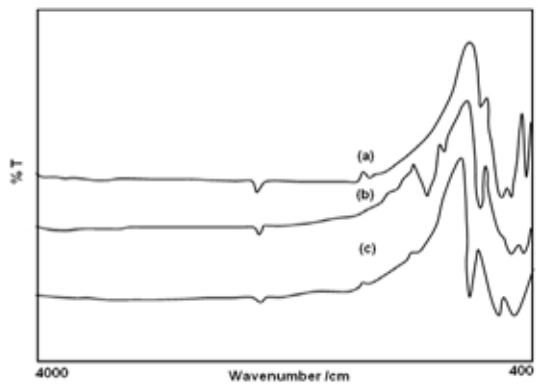

Fig. 1 IR spectra of synthesized photocatalyst a) $PbZrO_3$, b) $CdZrO_3$, and $CuZrO_3$

Figure 2 depicts UV-visible diffused reflectance spectrum of synthesized photocatalyst. The band gap energy for $PbZrO_3$ (a), $CdZrO_3$ (b) and $CuZrO_3$ (c) are 4.66, 5.12 and 3.28 eV respectively.

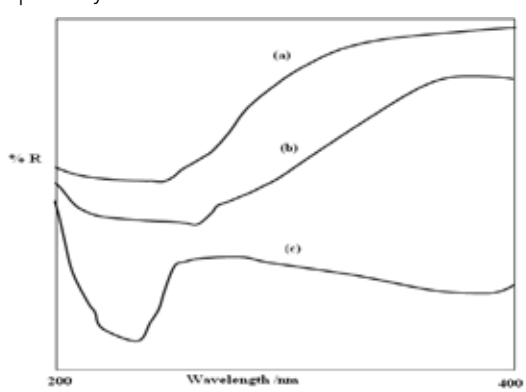

Fig. 2 UV-DRS spectra of synthesized photocatalyst a) $PbZrO_3$, b) $CdZrO_3$, and $CuZrO_3$

Figure 3 reveals XRD spectra of the synthesized photocatalyst. Figure 3(a) indicate XRD spectrum of $PbZrO_3$, the peaks in the spectrum at 2 theta matches well with the peaks in the JCPDS data card no. 35-0739. The peaks at an angle 21.3, 30.5, 37.6, 43.5, 54.1 angles indicate [021], [221], [240], and [261] planes confirming orthorhombic phase. Figure 3(b) shows XRD spectrum of $CuZrO_3$, The spectrum well matches with JCPDS data card no- 43-0953. The peaks in the spectrum at an angle of 24.19, 28.15, 34, 21, 40.84, 57.24 indicates [020], [112], [013], [023] and [400] planes confirming orthorhombic phase of the $CuZrO_3$. Figure 3(c) represent XRD spectrum of $CdZrO_3$. The spectra matches with the JCPDS data card no 84-0549. The plane at an angle 30.13, 34.91, 50.20, 59.66 etc are matches with the [111], [200], [220], and [311] planes. Grain size was calculated by Scherer's method and found to be 35.68 nm for $PbZrO_3$, 28.54 nm for $CdZrO_3$ and 26.54 for $CuZrO_3$.

Volume : 3 | Issue : 7 | July 2013 | ISSN - 2249-555X

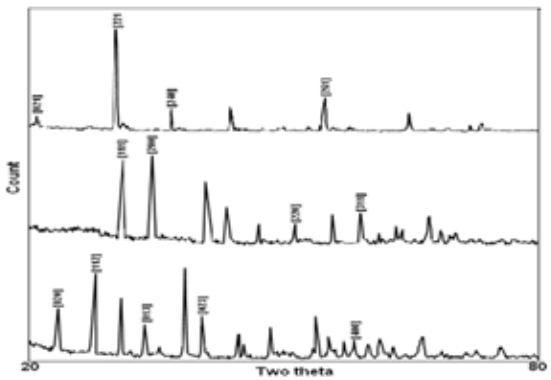

Fig. 3 XRD pattern of synthesized photocatalyst a) $PbZrO_3$, b) $CdZrO_3$, and $CuZrO_3$

Figure 4 (a), 4 (b) and 4 (c) shows surface morphology SEM along with EDAX of the synthesized photocatalysts $PbZrO_3$, $CdZrO_3$ and $CuZrO_3$ respectively. The SEM image depicts that all photocatalyst are crystalline in nature and particles are well agglomerated with each other uniformly distributed. The EDAX analysis was employed to determine the composition of the photocatalyst. The EDAX data furnishes information about confirming elemental composition taken for the synthesis.

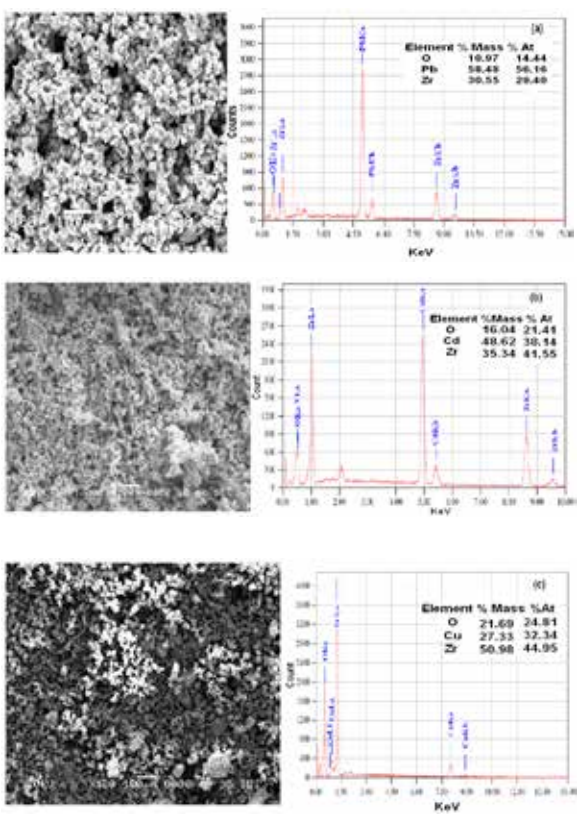

Fig. 4 SEM with EDAX of a) $PbZrO_3$, b) $CdZrO_3$, and $CuZrO_3$

Figure 5 (a-c) represents TEM image along with SAED pattern of synthesized photocatalysts. Figure 5 (a) image reveals that the particles are well distributed and shows orthorhombic structure. The SAED pattern associated with the dark spot reveals occurrence of $PbZrO_3$ orthorhombic structure with good agreement with XRD pattern. The dark spot at the distance of 3.42, 4.21 and 4.83 nm^{-1} indicate [221], [240], and [261] plane at 30.56, 37.79 and 43.67 degree respectively. Figure 5 (b) indicate the TEM image with SEAD pattern of $CuZrO_3$. The figure depicts that the particles are crystalline with orthorhombic structure. The SAED pattern associated with dark spot reveals occurrence of orthorhombic structure with good agreement with XRD pattern of $CuZrO_3$. The dark spot at a distance of 4.52 and 5.52 nm^{-1} indicate [023], and [440] planes at an angle 40.84 and 57.24 respectively. Similarly Figure 5 (c) TEM image with SAED pattern of $CdZrO_3$. The TEM image reveals that the particles are orthorhombic in nature. The SAED pattern associated with dark spot at the distance of 3.71 and 5.52 nm-1 indicate [111], and [220] planes at an angle of 34.91 and 50.20 respectively.

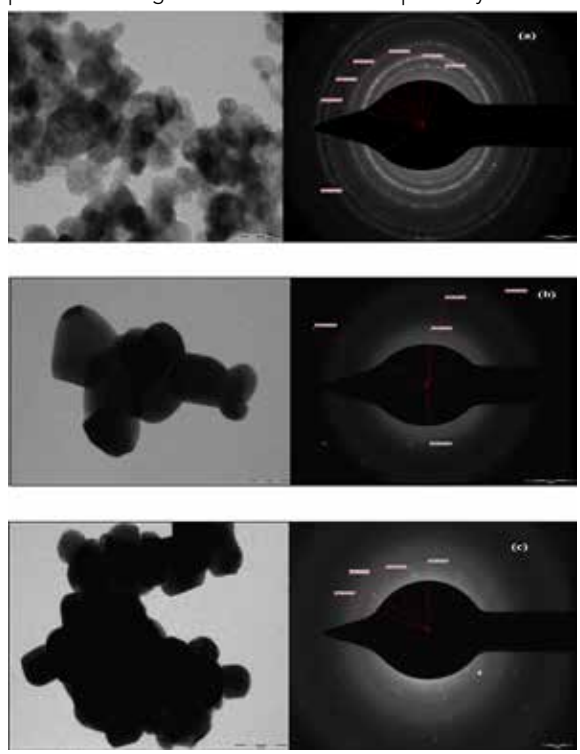

Fig. 5 TEM with SAED pattern of a) $PbZrO_3$, b) $CdZrO_3$, and $CuZrO_3$

Figure 6 (a), 6 (b) and 6 (c) represents the N_2 adsorption desorption isotherm of synthesized $PbZrO_3$, $CdZrO_3$, and $CuZrO_3$ respectively. It ravels that, all synthesized photocatalyst have typical H1 hysteresis curve, which indicates that, all samples have a narrow pore diameter range. From BJS adsorption desorption isotherm and BET surface area, for $PbZrO_3$ the surface area (S_{BET}) is 49.49 m^2/g pore volume (Vp) is 0.05411 cc/g and pore diameter (Dp) is 24.85 A° For $CdZrO_3$, the surface area (S_{BET}) is 13.60 m^2/g pore volume (Vp) is 0.0298 cc/g and pore diameter (Dp) is 24.85 A°. For $CuZrO_3$, the surface area (S_{BET}) is 20.22 m^2/g pore volume (Vp) is 0.0811 cc/g, and pore diameter (Dp) is 30.39 A°. Electrical performance hence energy of activation of the materials were studied by measuring change in conductance with temperature.

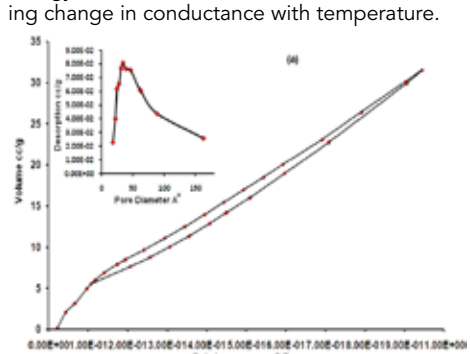

Volume : 3 | Issue : 7 | July 2013 | ISSN - 2249-555X

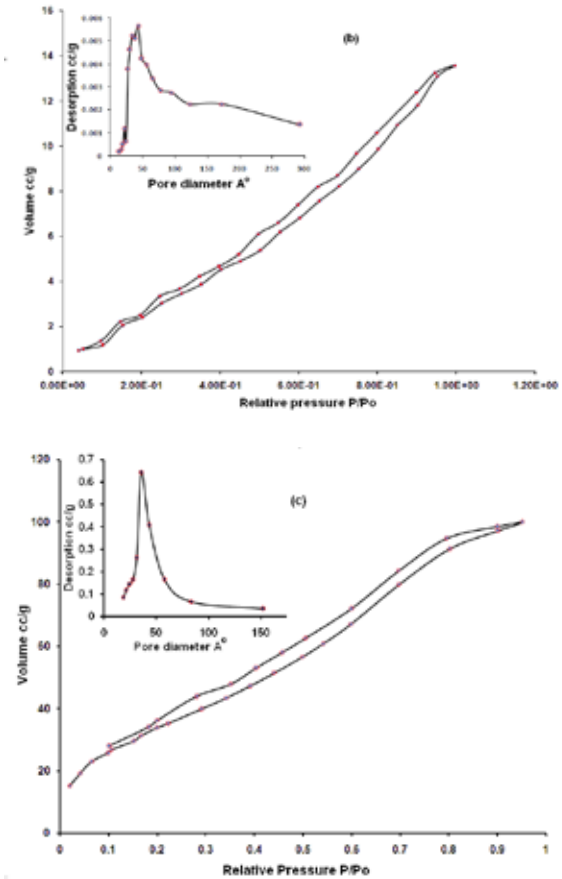

Fig. 6 BET Surface area a) $PbZrO_3$, b) $CdZrO_3$, and $CuZrO_3$

Fig. 7 (a), 7(b) and 7 (c) shows the dependence of conductivity of film in air ambience. The conductivity of the film goes on increasing with increase in temperature, showing semiconducting nature of the film.

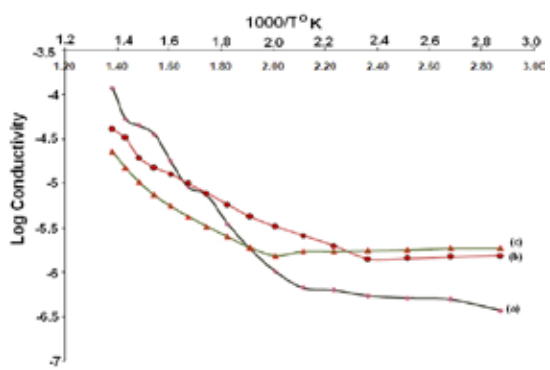

Fig. 7 Electrical conductivity of a) $PbZrO_3$, b) $CdZrO_3$, and c) $CuZrO_3$

The activation energy, the energy required to promote photoelectrons from the photo catalyst to be trapped at surface by adsorbed oxygen molecules for $PbZrO_3$, $CdZrO_3$ and $CuZrO_3$ were of the synthesized materials were found to be 9.97, 4.42 and 3.47 KJ/mole respectively. The observed trend in activation energies is in reverse order of ionic radii smaller ion carries more current and hence shows decrease in activation energy. The thermal stability of the photocatalysts were evaluated by thermogravimetric study as shown in Fig 8 curve (a-c). The photocatalyst was found to be very stable over wide range of the temperature.

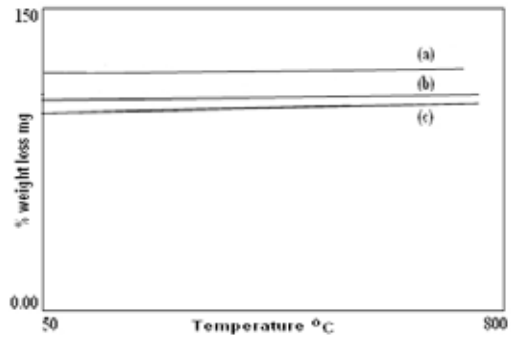

Fig. 8 Thermogravimetric plot of photocatalyst a) $PbZrO_3$, b) $CdZrO_3$, and c) $CuZrO_3$

2.2 Photodegradation study

The Figure 9 (a) represents the photocatalytic degradation of the direct black dye with 0.250 gm of $PbZrO_3$ photocatalyst. The figure shows that the absorption due to the chromophoric peak of dye solution was decreased with time in presence of the sunlight indicating degradation of dye. Figure 9 (b) represents the photocatalytic degradation of the direct black dye with 0.250 gm of $CdZrO_3$ photocatalyst. Figure 9 (c) represents the photocatalytic degradation of the direct black dye with 0.250 gm of $CuZrO_3$ photocatalyst. Figure 9 indicate the percentage degradation over time.

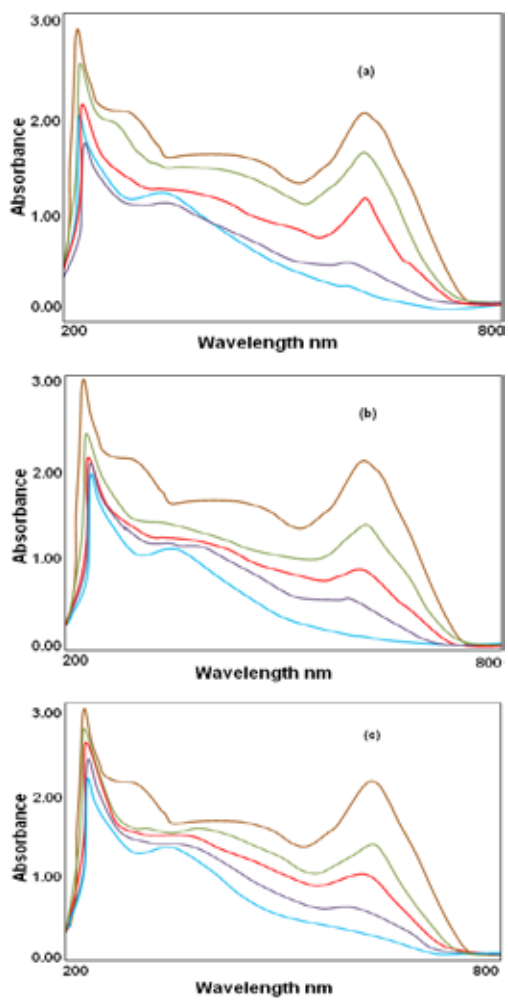

Fig. 9 UV-visible spectra of dye with a) $PbZrO_3$, b) $CdZrO_3$, and $CuZrO_3$

Volume : 3 | Issue : 7 | July 2013 | ISSN - 2249-555X

In the figure 10, curve-a, indicate degradation of direct black dye solution in presence of $CuZrO_3$ photocatalyst. Curve-b indicates degradation of direct black dye solution in presence of $CdZrO_3$ photocatalyst. The curve-c indicates degradation of dye solution in presence of $PbZrO_3$ In the figure; curve-d indicates degradation of dye solution when exposed to the sunlight in absence of photocatalyst. The curve-e indicates the effect of photocatalyst when dye solution was kept in the dark. The rate of degradation of direct black dye by using $CuZrO_3$ is found maximum than other two because of activation energy of $CuZrO_3$ is lower than other two.

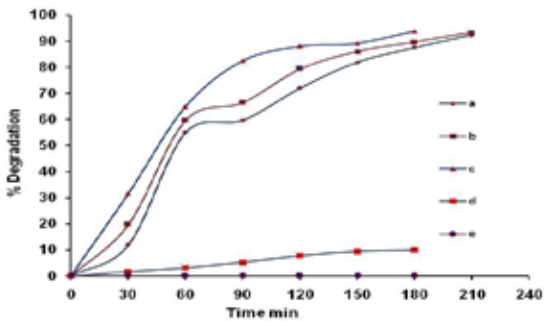

Fig. 10 Percentage degradation of direct black dye

The photocatalytic degradation of the dye is believed to take place according to the following mechanism. When a catalyst is exposed to UV radiation, electrons are promoted from the valence band to the conduction band. As a result of this, an electron–hole pair is produced.

$MZrO_3 + h\nu \rightarrow e^-$ (conduction band) + h^+ (Valence band) (1)

(Where M= Pb, Cd and Cu)

Where, e^- (conduction band) and h^+ (valance band) are the electrons in the conduction band and the electron vacancy in the valence band, respectively. Both of these entities migrate to the catalyst surface, where they can enter in a redox reaction. In the most the cases h+ (valance band) react easily with surface bound H_2O to produce •OH radicals, whereas e^- (conduction band) react with O_2 to produce superoxide, $O^{2-\bullet}$ radical anion of the oxygen

$H_2O + h^+$ (valance band) $\rightarrow$ •OH + H^+ (2)

$O_2 + e^-$ (conduction band) $\rightarrow O^{2-\bullet}$ (3)

This reaction prevents the combination of the electron and the hole, which are produced in the first step. The •OH and $O^{2-\bullet}$ produced in the above manner can then react with the Dye to form other species and is thus responsible for the degradation.

$O^{2-\bullet} + H_2O \rightarrow H_2O_2$ (4)

$H_2O_2 \rightarrow 2\bullet OH$ (5)

$\bullet OH + Dye \rightarrow Dye\ ox$ (6)

Dye + e^-(conduction band) $\rightarrow$ Dye red (7)

It may be noted that, all these reaction in the photocatalysis are possible due to the presence of both dissolved oxygen and water molecules. The rate of degradation of dye solution was evaluated and found to follow first order kinetics as shown in Fig. 11. Curve-a, b and c indicate rate of degradation of direct black by using $PbZrO_3$, $CdZrO_3$ and $CuZrO_3$. The observed rate constant for $PbZrO_3$, $CdZrO_3$ and $CuZrO_3$ are 0.0115, 0.0115 and 0.013 min^{-1} respectively.

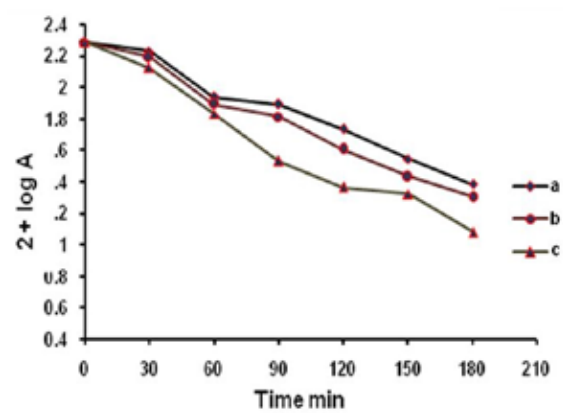

Fig. 11 Kinetic study of degradation of direct black dye

4. Conclusions

The light-driven photocatalyst $PbZrO_3$, $CdZrO_3$ and $CuZrO_3$ were synthesized by eco-friendly mechanochemical method. The photodegradation of direct black dye follows pseudo first order kinetics. The band gap energies for $PbZrO_3$, $CdZrO_3$ and $CuZrO_3$ are 4.66, 3.28 and 5.12 respectively. The activation energy for the synthesized photocatalyst observed to be3.70, 1.987 and 1.51 KJ/mole respectively. The rate of degradation of $CuZrO_3$ was found to be higher than $CdZrO_3$ and $PbZrO_3$.

6. Acknowledgements

This work was supported by the University Grants Commission, New Delhi, India, under Research programme. We are grateful to Head, Department of Physics, Indian Institute of Technology, Mumbai, India, for X-ray diffractrogram characterization techniques for analysis. Analysis

Volume : 3 | Issue : 7 | July 2013 | ISSN - 2249-555X

REFERENCE

[1] Tsuda, S., Murakami, M., Matsusaka, N., Kano, K., Taniguchi K., and Sasaki, Y., (2001) DNA Damage Induced by Red Food Dyes Orally Administered to Pregnant and Male Mice. Toxicological Sciences, 61(1): 92-99. DOI: 10.1093/toxsci/61.1.92. | [2] Garg, V., Gupta, R., Yadav, A., and Kumar, R., (2003) Dye removal from aqueous solution by adsorption on treated sawdust. Bioresource Technology, 89(2) 12 DOI.org/10.1016/j.biortech.2004.07.011. | [3] Bohdziewicz, J., Sroka, E., and Korus, I., (2003) Application of ultrafiltration and reverse osmosis to the treatment of the wastewater produced by the meat industry. Polish Journal of Environmental Studies, 12 (3) 269-274. | [4] Gholami, M., and Nasser, S., (2001) Dye Removal from Effluents of Textile Industries by ISO9888 Method and Membrane Technology. Iranian Journal of Public Health, 30(1-2) 73-80. | [5] Ohnishi, M., and Okuno,Y., (1998) Decoloration system using rotating membrane UF module, Water Science and Technology, 38(6) 35-43. | [6] Moghaddam, S., Alavi, M., and Arami, M., (2010) Coagulation/flocculation process for dye removal using sludge from water treatment plant: Optimization through response surface methodology. Journal of Hazardous Materials, 175 (1-3) 65-657. DOI.org/10.1016/j.jhazmat.2009.10.058. | [7] Stolz, A., (2001) Basic and applied aspects in the microbial degradation of azo dyes. Applied Microbiology and Biotechnology, 56(1-2) 69-80. DOI- 10.1007/s002530100686. | [8] Chu, W., and Wai, C., (2000) Quantitative prediction of direct and indirect dye ozonation kinetics. Water Research, 34(12): 3153-3160. DOI.org/10.1016/S0043-1354(00)00043-9. | [9] Manilal, V., Haridas, A., Alexander, R, and Surender, G., (1992) Photocatalytic treatment of toxic organics in wastewater: Toxicity of photodegradation products. Water Research, 26(81035-1038. DOI.org/10.1016/0043-1354(92)90138-T. | [10] Diana, V., (2007) Microbial toxicity of pesticide derivatives produced with UV photodegradation. Bulletin of Environmental Contamination and Toxicology, 79, 356-359. 10.1007/s00128-007-9230-7. | [11] Ioannis, K., and Triantafyllos, A ., (2003) Photocatalytic transformation of pesticides in aqueous titanium dioxide suspensions using artificial and solar light: intermediates and degradation pathways. Applied catalysis- B, 42(4) 319-335. DOI.org/10.1016/S0926-3373(02)00266-7. | [12] Kitsiou, V., and Filippidis, N., (2009) Heterogeneous and homogeneous photocatalytic degradation of the insecticide imidaclopride in aqueous solution. Applied catalysis-B, 86 27-35. DOI.org/10.1016/j.apcatb.2008.07.018. | [13] Weisburger, J., (2002) Comments on the history and importance of aromatic and heterocyclic amines in public health. Mutation Research, 506-507, 9-20. DOI.org/10.1016/S0027-5107(02)00147-1. | [14] Borhade, A., and Baste, Y., (2012) Green chemistry approach for the synthesis of PbSnO3: An effective photocatalyst for the degradation of dyes under sunlight. Journal of Thermal Analysis and Calorimetry, 107 77-83. 10.1007/s10973-011-1672-9. | [15] Fabiola, M., Santiago, E., and Jaime G., (2010)Degradation of immerging contaminant ibuprofen in water by photofenton. Water research, 44 589-595 DOI.org/10.1016/j.watres.2009.07.009. | [16] Doggan, H., Shijun, L., and Shuiqing, Q., (2007) Preparation of anatase F doped TiO2 sol and its performance for photodegradation of formaldehyde. Journal of Materials Science, 42(19) 8193-8202. DOI. 10.1007/s10853-007-1694-7. | [17] Vulliet, E., and Emmelin, C., (2003) Photocatalytic degradation of herbicide cinosulfuron in aqueous TiO2 suspension. Environmental Chemistry Letters, 3(1) 62-67. DOI 10.1007/s10311-002-0008-1. | [18] Behnajady, M., Modirshahla, N., and Hamzavi, R., (2006) Kinetic study on photocatalytic degradation of C.I. Acid Yellow 23 by ZnO photocatalyst. Journal of Hazardous Materials, 133(1-3) 226-232. DOI.org/10.1016/j.jhazmat.2005.10.022. | [19] Tada, H., and Hattori, A., (2000) Patterned-TiO2/SnO2 bilayer type photocatalyst. Journal of Physical Chemistry- B, 104(19) 4585-4587. DOI. 10.1021/jp000049r. | [20] Wang, C., (2004) Enhanced photocatalytic performance of nanosized coupled ZnO/SnO2 photocatalyst for methyl orange degradation. Journal of Photochemical and Photobiology- A, 168,47-52. DOI:10.1016/j.jphotochem.2004.05.014. | [21] Wang, W., Zhu, Y., and Yang, L., (2007) ZnO–SnO2 Hollow spheres and hierarchical nanosheets: hydrothermal preparation, formation mechanism, and photocatalytic properties. Advanced Functional Materials, 17(1) 59-64. DOI: 10.1002/adfm.200600431. | [22] Celik, E., and Gokcen, Z., (2006) Processing, characterization and photocatalytic properties of Cu doped TiO2 thin films on glass substrate by sol–gel technique. Journal of Material Science and Engineering-B, 132(3) 258-265. doi.org/10.1016/j.mseb.2006.03.038. | [23] Borhade, A., Kanade, K., Tope, D., and Patil, M., (2012) A Comparative study on synthesis, characterization and photocatalytic activities of MgO and Fe/MgO nanoparticles. Research on Chemical Intermediate, 38(8) 1931-1946. DOI: 10.1007/s11164-012-0515-z. | [24] Subramanian, V., Roeder, R., and Wolf, E., (2006) Synthesis and UV−Visible-Light Photoactivity of Noble-Metal−SrTiO3 Composites. Industrial and Engineering Chemistry Research, 45 (7) 2187-2193. DOI: 10.1021/ie050693y. | [25] Aramendía, M., (2005) Photocatalytic degradation of herbicide fluroxypyr in aqueous suspension of TiO2. Catalysis Today. 101 187-193. DOI: 10.1016/j.cattod.2005.03.063. | [26] Song, Z., and Wang, S., (2004) Synthesis of manganese titanate MnTiO3 powders by a sol–gel–hydrothermal method. Materials Science and Engineering: B, 113(2) 121-124. DOI.org/10.1016/j.mseb.2004.06.002. | [27] Zoltan, A., Nandor, B., Tunde, A., Gyula, W., Pal, S., Andras, D., and Karoly, M., (2008) Synthesis, structure and photocatalytic properties of Fe(III)-doped TiO2 prepared from TiCl3. Applied catalysis, B, 81 27-37. DOI:10.1016/j.apcatb.2007.11.041. | [28] Natarajan, N., and Nogami, G., (1998) Titanium dioxide thin film deposited by spray pyrolysis of aqueous solution. Thin Solid Films, 322(1–2) 6-8. DOI:10.1016/S0040-6090(97)01010-9. | [29] Sun, H., and Akpan, C., (2008) Photocatalytic TiO2 films prepared by chemical vapor deposition at atmosphere pressure. Journal of Non-Crystalline Solids, 354, 1440-1443. DOI:10.1016/j.jnoncrysol.2007.01.108. |